Available online at www.sciencedirect.com
ScienceDirect
Journal of Power Sources 180 (2008) 657–663
JOURNAL OF POWER SOURCES
www.elsevier.com/locate/jpowsour

Improving power density and efficiency of miniature radioisotopic thermoelectric generators

Scott A. Whalen *, Christopher A. Apblett, Terrence L. Aselage

Sandia National Laboratories, Albuquerque, NM 87185, USA

Received 12 December 2007; received in revised form 16 January 2008; accepted 22 January 2008
Available online 14 February 2008

Abstract

We have built and tested a prototype miniaturized thermoelectric power source that generates 450 μW of electrical power in a system volume of 4.3 cm^3. The measured power density of 104 μW cm^{-3} exceeds that of any previously reported thermoelectric power system of equivalent size. This improvement was achieved by implementing a novel thermopile design in which wagon wheel-shaped thermoelectric elements contact the entire circumference of the heat source whereas traditional approaches utilize only one heat source surface. The thermopile consists of 22 wagon wheel-shaped elements (11 P–N thermocouples) fabricated from 215-μm thick bismuth–telluride wafers having ZT = 0.97 at 30 °C. The power source operates on a 150 mW thermal input provided by an electrical resistance heater that simulates a capsule containing 0.4 g of $^{238}PuO_2$ located at the center of the device. Our primary research objective was to develop and demonstrate a prototype thermopile and radioisotopic thermoelectric generator (RTG) architecture with improved power density at small scales. Output power from this device, while optimized for efficiency, was not optimized for output voltage, and the maximum power was delivered at 41 mV. We also discuss modifications to our prototype design that result in significantly improved voltage and power. Numerical predictions show that a power output of 1.4 mW, power density of 329 μW cm^{-3}, and voltage of 362 mV, is possible in the same package size.

Keywords: RTG; Thermopile; Thermoelectric; Miniature; Power density; Efficiency

1. Introduction

For power source applications requiring small volume and decades of operation where harvestable energy is unavailable, only devices that convert radioactive decay into electricity can provide high energy densities. As a result, a variety of nuclear-based small-scale power sources have been developed with varying degrees of success and maturity. The most successful approaches employ indirect conversion of alpha or beta emissions into electricity using thermoelectric [1], thermoacoustic [2], thermionic [3], thermophotovoltaic [4], betavoltaic [5], alphavoltaic [6], and piezoelectric [7] methods. Direct conversion of beta particles has also been proposed in the literature for direct charging [8] but practical devices have not been realized. Of all the approaches mentioned, the most reliable and power dense miniature power sources have proven to be RTGs developed for biomedical applications [9,10].

The smallest commercially fielded RTGs were developed in the late 1960s and early 1970s for use as power sources in cardiac pacemakers [11]. From 1970 to 1984, over 3000 RTGs, using $^{238}PuO_2$ as the heat source, were implanted worldwide achieving an extremely high safety and reliability record [12]. Table 1 shows a summary of the beginning of life (BOL) characteristics for high performance implantable miniature RTGs. These RTGs all have significant design variations with each approach using a different combination of fuel loading, fibrous vs. multifoil insulation, spring vs. hard contact compression, and bismuth–telluride vs. silicon–germanium thermoelectric materials. However, the basic geometric arrangement of the main internal components is the same. All RTGs described in Table 1 utilize thermal insulation surrounding a plutonium heat capsule that is compressed in linear fashion against a parallelepiped monolithic thermopile.

Based on the prevalence of this approach, it is evident that Raag is correct in stating that "the configuration that has

* Corresponding author. Tel.: +1 505 845 2040; fax: +1 505 844 6972.
E-mail address: sturgeonguy@hotmail.com (S.A. Whalen).

0378-7753/$ – see front matter © 2008 Elsevier B.V. All rights reserved.
doi:10.1016/j.jpowsour.2008.01.080

Table 1
Summary of BOL performance for implantable RTGs

Manufacturer	Voltage (V)	Power (μW)	Volume (cm^3)	Power density ($\mu W\,cm^{-3}$)	Efficiency (%)
Nuclear Battery Corp. [13,14]	0.3	600	11	55	0.75
General Atomic [13,14]	0.4	400	8	50	0.40
Syncal [13,14]	5.0	300	5	60	0.40
CIT-Alcatel [13,14]	0.6	250	19	13	0.35
Russian TEB [15]	5.0	500	8	63	0.33

been almost universally adopted is a parallelepiped monolithic [thermopile] structure located at one or both ends of a cylindrical fuel capsule [16].” However, Raag interestingly asserts that this configuration is not optimal. “An optimum configuration would appear to be washer-shaped [thermoelectric elements] modules located around the periphery of a cylindrical fuel capsule.” Raag then explains why this configuration has not been used in practice. “Although such an arrangement possesses good mechanical strength, the required output power and voltage can only be achieved if the thermoelements are extremely thin, less than 0.001 in. (25 μm).” These statements identifying a more optimal configuration motivated our investigation of alternative thermopile structures and device geometries.

The primary objective of our initial research phase, reported herein, was to develop and demonstrate a prototype thermopile and RTG architecture with improved power density at small scales. We chose power density as the critical parameter based on our interest in reducing power source volume, extending mission life, and facilitating higher power applications. We focused largely on power density at the expense of operating voltage with the intention of increasing voltage during future design iterations. Our objectives during this phase of development did not include engineering a field ready nuclear device, but centered around exploring and developing an alternative geometry with a power density superior to existing small scale RTGs. In this paper we report the results of our progress toward achieving this goal.

2. Model approach

To accomplish our goal of increased power density, we first developed a simple 1D-coupled thermoelectrical model as a tool for exploring different thermopile and RTG architectures. Predictions for efficiency, power density, and voltage were used to identify the RTG design presented herein. Fig. 1 is a schematic of the model and shows the division of heat flowing from the heat source, Q_{HS}, to the RTG container, Q_{CAN}. Q_{LOSS} accounts for heat losses, such as conduction through the insulation, which completely bypass the thermopile. Q_H and Q_C represent the heat flowing into and out of the thermopile with hot and cold junction temperatures T_{HJ} and T_{CJ}. Taking a control volume around the thermopile, defined by the dashed red box, and performing an energy balance, yields the expression in Eq. (1). This equation simply states that the difference between heat flowing into and out of the thermopile is equal to the electrical power generated, where I is current and R_L is the load resistance:

$$Q_H - Q_C = P_{OUT} = I^2 R_L \tag{1}$$

Performing an energy balance around the yellow boxes at the hot and cold junctions of the thermopile yields expressions for Q_H and Q_C as shown in Eqs. (2) and (3). In these equations, Q_{INS} and Q_K are conduction heat flow through the dielectric insulator between and thermoelectric elements, respectively, Q_P is Peltier heating and cooling, Q_J is Joule heating, and Q_T is Thompson heating. Also included in these equations is Joule heating, Q_{Jcont}, within the electrical interconnects between thermoelectric elements:

$$Q_H = Q_K + Q_{INS} + Q_{PH} - \tfrac{1}{2}Q_J - \tfrac{1}{2}Q_T - Q_{JcontH} \tag{2}$$

$$Q_C = Q_K + Q_{INS} + Q_{PC} + \tfrac{1}{2}Q_J + \tfrac{1}{2}Q_T + Q_{JcontC} \tag{3}$$

The heating and cooling associated with thermoelectric effects can be collected into the terms Q_{TEH} and Q_{TEC} at the hot and cold junctions and Eqs. (3) and (4) can be rewritten as Eqs. (4) and (5):

$$Q_H = Q_K + Q_{INS} + Q_{TEH} \tag{4}$$

$$Q_C = Q_K + Q_{INS} + Q_{TEC} \tag{5}$$

An interesting result is observed in Eq. (6), which shows the outcome of substituting Eqs. (4) and (5) into Eq. (1). This shows that the difference in the thermoelectric heating and cooling at the hot and cold junctions is equal to the power generated by the thermopile:

$$Q_{TEH} - Q_{TEH} = I^2 R_L \tag{6}$$

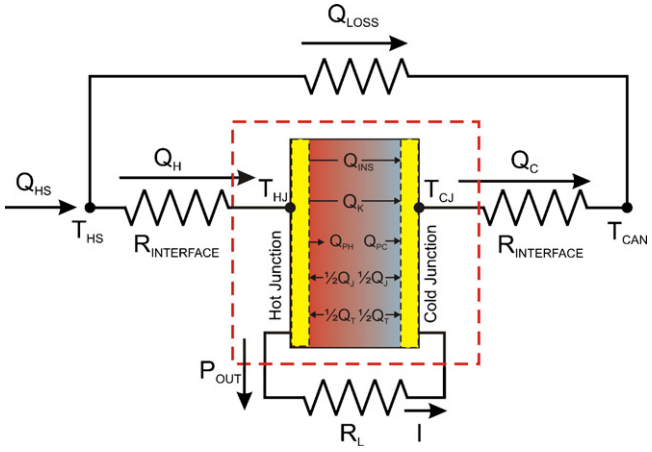

Fig. 1. Schematic of 1D thermoelectrical model.

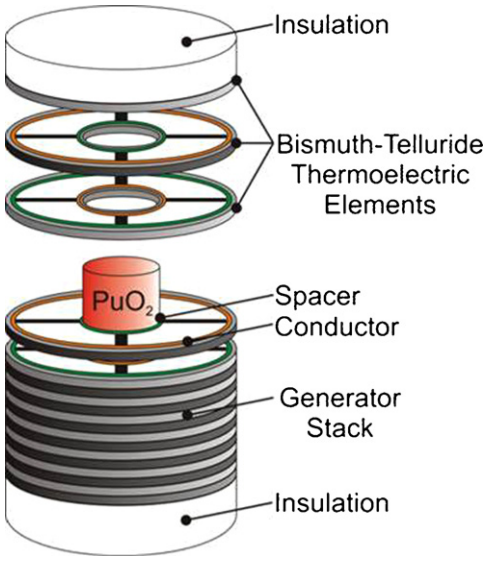

Fig. 2. Conceptual design of miniature RTG.

In this paper we will not describe the full theoretical development and numerical procedure used to solve the above system of equations. In short, an iterative technique is used to solve the above system of equations for the unknown nodal temperatures and current flow. This simple model allowed for quick investigation and comparison of different RTG and thermopile geometries and guided the design presented herein.

3. Design and fabrication

After examining multiple device configurations using our simple 1D model, we also determined that the optimum configuration, in terms of power density and efficiency, consists of washer-like thermoelectric elements wrapped around the perimeter of a cylindrical fuel capsule. This is primarily due to the fact that a larger portion of the heat source can be covered with thermoelectric material as compared to the typical linear parallelepiped design. In fact, for this configuration, efficiency increases as the cylinder becomes longer because the thermal resistance of the end cap insulation is fixed and independent of the device length. This results in more heat passing through the thermopile as the thermoelectric stack becomes taller. As a result, we proceeded to design a prototype miniature RTG implementing this radial approach. Our miniature RTG concept, shown in Fig. 2, consists of a heat source capsule wrapped with wagon wheel-shaped thermoelectric elements. Thermal insulation for channeling heat through the thermopile is provided by insulating disks at opposite faces of the structure. Although vacuum multifoil insulation provides greater insulation than fibrous materials, solid Min-K was used in our prototype for the purpose of simplifying RTG assembly and avoiding the challenges associated with maintaining hard vacuum for decades of operation.

An electrically heated surrogate was used in the prototype to simulate a 150 mW $^{238}PuO_2$ fuel pellet. In determining the size of the capsule and volume of fuel necessary we assumed an isotopic enrichment of 83%, theoretical density of 86%, and power

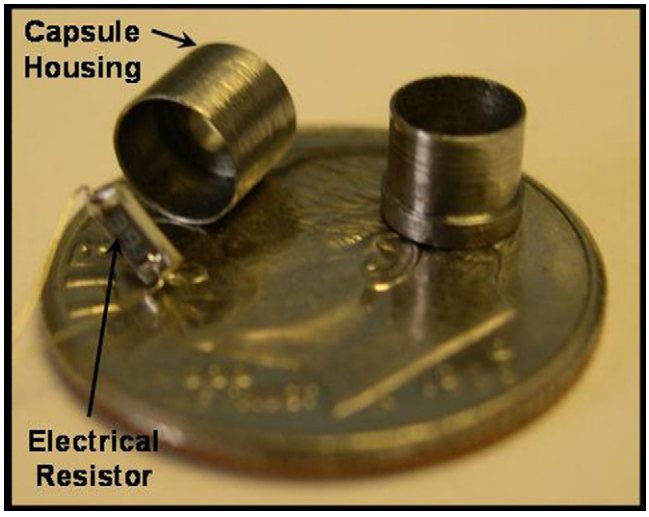

Fig. 3. Surrogate heat source.

density of 3.9 W cm^{-3}, which are representative of $^{238}PuO_2$ fuel used in previous biomedical applications [17]. A 150 mW heat source would require a fuel volume of 0.038 cm^3 having a mass of 0.4 g and activity of 5.5Ci. The stainless steel surrogate, shown in Fig. 3, measures 5 mm in length, 4.2 mm in diameter, with an interior volume of 0.038 cm^3. For testing purposes, the surrogate heat source contains a 390 Ω surface mount resistor packed in aluminum oxide (Al_2O_3). DC current was applied to the resistor to simulate heat generated by a $^{238}PuO_2$ fuel capsule. We recognize the rigor inherent in designing a field ready heat source; however, this paper focuses on developing a new device architecture and not engineering a field ready unit.

Heat is converted into electricity through our unique thermopile geometry using P and N type Bi_2Te_3 with ZT optimized for an average operating temperature of 30 °C. Rather than solid washers, our modeling indicates that the spoked configuration shown in Fig. 4 would yield higher device efficiency. This is because the spoked design increases the thermal resistance of the elements, as compared to a solid washer, thereby increasing the temperature difference and efficiency.

Fabrication of the spoked elements begins with dicing bulk Bi_2Te_3 ingots into thin rectangular plates measuring 7.6 cm × 2.5 cm × 215 μm as shown in Fig. 5. The plates are then stacked and aligned within a jig and wire electron discharge machining (EDM) is used to simultaneously cut out the spoked

Fig. 4. Spoked P and N type thermoelectric elements.

Fig. 5. 215-μm thick Bi_2Te_3 plates.

elements. The resulting wagon wheel-shaped thermoelectric elements have an i.d. = 4.4 mm and o.d. = 15 mm with each of the four spokes measuring 3.2 mm × 500 μm × 215 μm. The spokes are then masked and the inner and outer hubs are sputtered with a molybdenum diffusion barrier followed by gold to ensure ohmic contact between elements.

The thermopile is then constructed by alternately stacking the P and N type Bi_2Te_3 elements around a cylindrical jig having the same diameter as the surrogate heat source. During the stacking process, the elements are separated by inner and outer rings of two different 25 μm thick materials which provide electrical connections and structural support between TE layers. Electrical connections between elements are made using rings of gold-coated copper while structural support and electrical isolation are provided using rings of Kapton® polymer film, both shown in Fig. 6. The conductor/insulator materials alternate position for each level of the stack to maintain the necessary series connection between the P and N type elements as shown in Fig. 7. With the stack held in compression by a jig, a low viscosity epoxy is then wicked onto the interior surface of the inner hub and exterior surface of the outer hub and cured at room temperature. The jig is then released and the monolithic thermopile is complete as shown in Fig. 8. The surrogate heat source is then pressed into the thermopile to ensure good thermal contact and the terminal electrical connections shown in Fig. 6 are attached to each face of the thermopile. Min-K insulation disks are then placed on each face of the thermopile and the assembly is pressed into a stainless steel container to ensure good thermal contact between the cold junctions and container.

The resulting spoked thermopile contains 22 Bi_2Te_3 layers forming 11 P–N thermocouples with the hot junctions located at the inner radius and cold junctions at the outer radius. Thermal

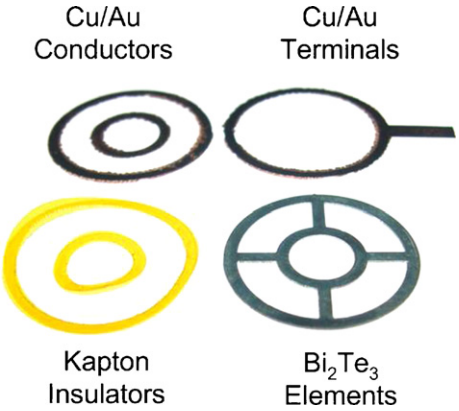

Fig. 6. Thermopile stack materials.

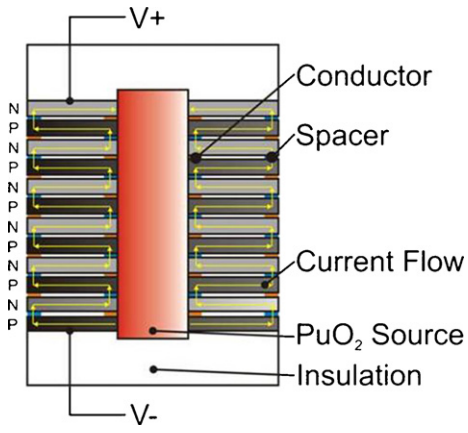

Fig. 7. Schematic of heat and current flow.

shunting is minimized in this design because the Bi_2Te_3 spokes are the only solid materials that fully bridge between the hot and cold junctions. Parasitic losses from the hot side to the cold side by conduction and convection are small due to the low thermal conductivity of the entrained air and extremely low Rayleigh number of the four gas pockets between spokes. In addition, radiative losses between the hot and cold junctions are minimal since the temperature difference between the hot and cold sides is small, on the order of 15 °C. The only two surfaces requiring insulation are located at the top and bottom faces of the cylindrical thermopile. Insulation is provided via 5 mm thick disks of Min-K TE1400 fibrous insulation ($k = 0.025\ W\ m^{-1}\ K^{-1}$) that force 70% of the heat in the radial direction. As a result, 65% of the total heat input flows through the spokes of the thermopile.

For the tests reported herein, the environment within the container is air at STP. The benefits of a lower thermal conductivity gas at modestly reduced pressure will be discussed later. Fig. 9 shows the assembled device with a section of the container cut away to allow for viewing of the internals. We chose a fibrous insulation rather than a hard vacuum and multifoil approach to

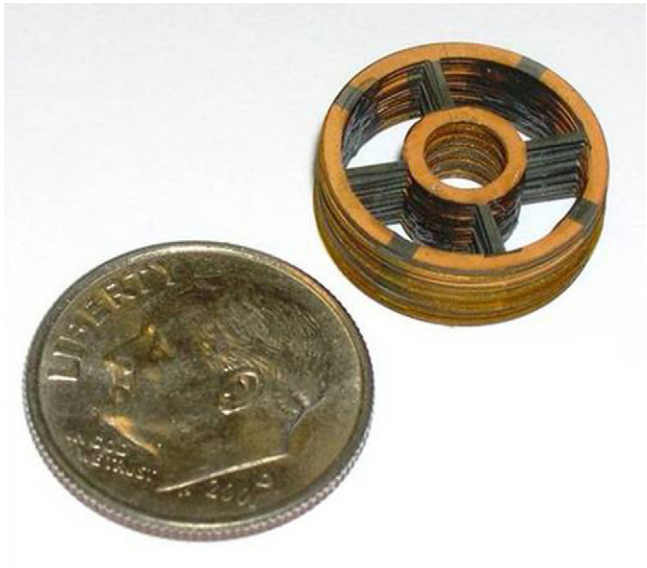

Fig. 8. Monolithic spoked thermopile with gold contacts visible.

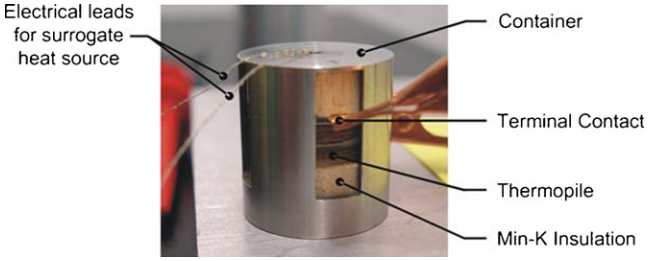

Fig. 9. Assembled prototype with cutout showing internals.

avoid the complexity and uncertainty of holding a sub-millitorr level vacuum for decades. In addition, the unique configuration of our design is such that compression of a fibrous insulation provides good mechanical strength. Fig. 10 shows the functional 4.3 cm^3 device next to a dime for scale. This version was fully enclosed, welded, and contained a miniature hermetic electrical feedthough.

4. Experimental and numerical results

Prior to electrical testing, the prototype was placed on an aluminum block and the leads from the surrogate heat source were connected to a precision digital power supply set to dissipate 150 mW within the surface mount resistor of the surrogate. We then waited for 24 h to ensure thermal equilibrium within the prototype. Electrical testing was then performed by sweeping values of a resistor connected in parallel with the thermopile while simultaneously measuring the resulting current flow and voltage across the resistor. Fig. 11 shows load voltage, current, and power generated by the prototype along with predictions

Fig. 10. Completed 4.3 cm^3 device with dime for scale.

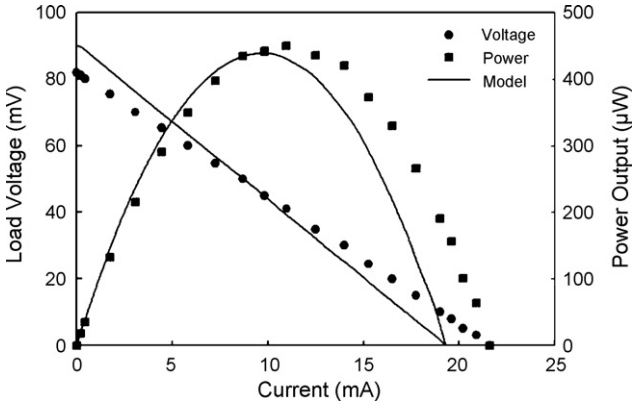

Fig. 11. Electrical performance of prototype compared to model predictions.

from the model. A peak power of 450 μW was generated at a load of 3.7 Ω corresponding to a power density of 104 μW cm^{-3}, current of 11 mA, voltage of 41 mV, and efficiency of 0.3%. The open-circuit voltage was measured at 82 mV which corresponds to a calculated $\Delta T = 15\,^{\circ}C$ across the thermopile while in the open-circuit condition.

This initial prototype compares favorably with the devices summarized in Table 1 especially in terms of power density and efficiency. Although efficiency and power density generally decrease as device size decreases, we achieved competitive power and power density from a system volume 46% smaller than the smallest miniature RTG found in the literature. Even though we achieved our primary goal of maximizing power density, the efficiency and especially the operating voltage must be improved if this architecture is to be become feasible as a real-world power source. A useful tool for determining these improvements is the 1D analytical model. Fig. 11 also shows that the model predicts the electrical performance relatively well in spite of the complicated 3D nature of the actual device. Although agreement between model and experiment is not exact for load resistances greater than the peak power, the simple model appears to be a useful tool for predicting the peak power, trends, and exploring design variables. Discrepancies between the data and model are most likely due to the assumptions and simplifications made to reduce the model to a 1D approximation of the device.

First, we explore the effect of backfilling the RTG container with xenon rather than air at STP. Xenon has a much lower thermal conductivity than air (0.006 $W\,m^{-1}\,K^{-1}$ vs. 0.027 $W\,m^{-1}\,K^{-1}$ at STP) and has the dual effect of reducing both parasitic heat losses through the gas pockets/layers of the thermopile and the thermal conductivity of the Min-K insulation [18]. We chose a modest vacuum of 40 Torr which reduces the Min-K thermal conductivity by a factor of two. Although an additional 10% reduction in Min-K thermal conductivity can be achieved using hard vacuum, we chose to avoid reliance on hard vacuum as stated previously. Fig. 12 shows the effect of changing the thermal conductivity of the gas pockets/layers within the thermopile from 0.027 to 0.006 $W\,m^{-1}\,K^{-1}$ and the thermal conductivity of the Min-K insulation from 0.025 to 0.012 $W\,m^{-1}\,K^{-1}$. A peak power of 882 μW is predicted

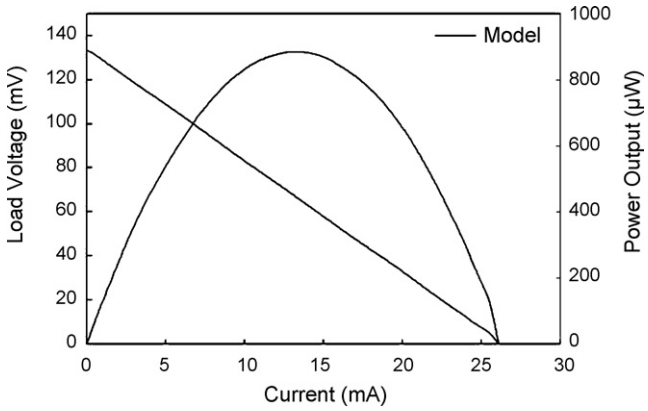

Fig. 12. Predicted electrical performance with 40 Torr xenon backfill.

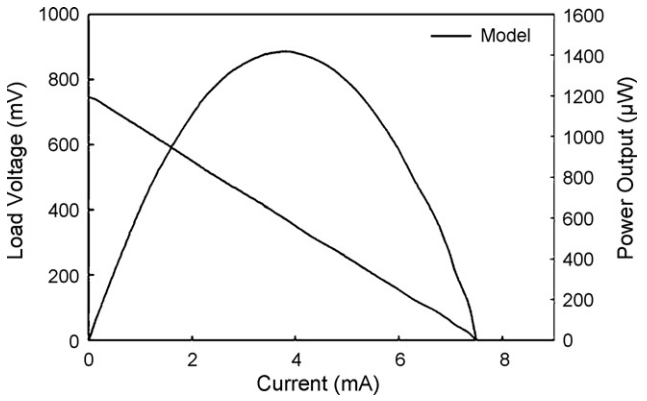

Fig. 14. Predicted electrical performance with xenon backfill, quartering, and 150-μm thick elements.

corresponding to a power density of 203 μW cm^{-3}, current of 12.5 mA, voltage of 71 mV, and efficiency of 0.6%. The predicted open-circuit voltage is 140 mV which corresponds to a calculated $\Delta T = 24\,^{\circ}$C across the thermopile while in the open-circuit condition. The model shows that backfilling the device with a modest 40 Torr vacuum of xenon is an effective means of boosting performance of the device.

Secondly, the thermopile geometry can be modified in two simple ways to improve both the operating voltage and efficiency. Recent manufacturing developments have revealed that the bulk Bi_2Te_3 plates shown in Fig. 5 can be thinned to 150 μm prior to EDM of the spoked thermoelectric elements. The thinner elements will increase the number of thermocouples from 11 to 14 while maintaining the same bulk thermopile dimensions resulting in a 27% increase in voltage. In addition to thinner elements, the voltage can also be boosted by quartering the thermopile, as shown in Fig. 13, and wiring the four sections in series. This configuration increases the number of couples from 14 to 56 and results in a fourfold increase in voltage.

Fig. 13. Quartered thermopile prior to re-bonding and series wiring.

Quartering the thermopile also improves efficiency because the electrical contact resistance between the thermoelectric elements and the Cu/Au conductors becomes a smaller percentage of the total thermopile resistance. By quartering the thermopile, the resistance of the thermoelectric elements increases by a factor of 16 but the contact resistance increase by only a factor of 4. This change in the ratio between contact and thermoelectric resistance results in an increase in power output for an equivalent heat flux. Fig. 14 shows the predicted cumulative effect of the 40 Torr xenon backfill, quartering the thermopile, and reducing the thickness of the thermoelectric elements from 215 to 150 μm. The cumulative effect of these design improvements results in a peak power of 1.4 mW corresponding to a power density of 329 μW cm^{-3}, current of 3.9 mA, voltage of 362 mV, and efficiency of 0.9%. The predicted open-circuit voltage is 752 mV which corresponds to a calculated $\Delta T = 24\,^{\circ}$C across the thermopile while in the open-circuit condition. If achieved, the power density would exceed that of the most power dense miniature RTG from Table 1 by a factor of 5 in a 46% smaller volume. The voltage is at the lower end of the values reported in Table 1 but is high enough for efficient DC–DC upconversion. Even accounting for an 80% efficient DC–DC boost circuit occupying 5 cm^3, the overall system would be 0.7% efficient with a power density of 120 μW cm^{-3}. In this case, the power density would still be a factor of two greater than the highest value from Table 1. However, internal work at SNL has shown that 80% efficient DC–DC upconversion is possible in a 1 cm^3 package.

5. Summary

The goal of this work was to realize a miniature RTG architecture that maximized power density and efficiency while simultaneously reducing system volume. This initial study demonstrates that our cylindrical design combined with a spoked thermopile has the potential to exceed the power density and efficiency of conventionally designed miniature RTGs. These potential improvements result primarily from the implementation of a unique design that allows for more efficient capture of heat from the heat source. Results from our first prototype show a power density of 104 μW cm^{-3} and efficiency of 0.3%. Reasonable modifications based on our simple 1D analytical model

predict a power density of 329 $\mu W\,cm^{-3}$, efficiency of 0.9%, voltage of 362 mV, in a volume of 4.3 cm^3. Such performance, if achieved, would constitute a significant advancement in the electrical performance of miniature RTGs.

Acknowledgment

This work was conducted at Sandia National Laboratories. Sandia is a multi-program laboratory operated under Sandia Corporation, a Lockheed Martin Company, for the United States Department of Energy under contract DE-AC04-94-AL85000.

References

[1] V. Raag, Proceedings of the 9th Intersociety Energy Conversion Engineering Conference, San Francisco, CA, January 1974, pp. 824–825.
[2] M. Petach, R. Tward, S. Backhaus, Design of a high efficiency power source (HEPS) based on thermoacoustic technology, Final Report, NASA Glenn Research Center, Contract no. NAS3 CDRL 3F, January 2004.
[3] V. Kornilov, Atom. Energy 91 (1) (2001) 586–589.
[4] V. Teofilo, P. Choong, Y. Tseng, Space Technology & Applications International Forum, Albuquerque, NM, February 2006, pp. 552–559.
[5] L. Olsen, Proceedings of the 12th Space Photovoltaic Research and Technology Conference, Cleveland, OH, 1993, pp. 256–267.
[6] S. Bailey, D. Wilt, S. Castro, C. Cress, R. Raffaelle, Proceedings of the Photovoltaic Specialists Conference, Lake Buena Vista, FL, January 2005, pp. 106–109.
[7] H. Guo, A. Lal, Proceedings of Transducers '03, Boston, MA, June 2003, pp. 36–39.
[8] A. Kononovich, M. Mitel'man, N. Rozenblyum, Atom. Energy 16 (6) (1964) 425–426.
[9] V. Parsonnet, Surgery 78 (6) (1978) 776–786.
[10] B. Owens, Batteries for Implantable Biomedical Devices, Plenum Press, New York, NY, 1986, pp. 335–336.
[11] B. Owens, Batteries for Implantable Biomedical Devices, Plenum Press, New York, NY, 1986, 345 pp.
[12] B. Owens, Batteries for Implantable Biomedical Devices, Plenum Press, New York, NY, 1986, pp. 348–350.
[13] D. Rowe, CDC Handbook on Thermoelectrics, CRC Press, Boca Raton, FL, 1995, 448 pp.
[14] A. Gasper, K. Fester, Proceedings of the 10th Intersociety Energy Conversion Engineering Conference, Newark, NJ, August 1975, pp. 1205–1213.
[15] A. Pustovalov, Proceedings of the 18th International Conference on Thermoelectrics, Baltimore, MD, August 1999, pp. 509–520.
[16] V. Raag, Proceedings of the 11th Intersociety Energy Conversion Engineering Conference, vol. 2, State Line, NV, September 1976, pp. 1586–1590.
[17] B. Owens, Batteries for Implantable Biomedical Devices, Plenum Press, New York, NY, 1986, pp. 290–295.
[18] A. Skrabek, R. Tye, A. Desjarlais, Rev. Int. Hautes Temp. Refract. 16 (4) (1979) 361–370.